Retigabine, a potassium channel opener, restores thalamocortical neuron functionality in a murine model of autoimmune encephalomyelitis

Luca Fazio, Venu Narayanan Naik, Rajeevan Narayanan Therpurakal, Fiorella M. Gomez Osorio, Nicole Rychlik, Julia Ladewig, Michael Strüber, Manuela Cerina, Sven G. Meuth, Thomas Budde

Suggested Citation:
Fazio, L., Naik, V. N., Narayanan Therpurakal, R., Gomez Osorio, F. M., Rychlik, N., Ladewig, J., Strüber, M., Cerina, M., Meuth, S., & Budde, T. (2024). Retigabine, a potassium channel opener, restores thalamocortical neuron functionality in a murine model of autoimmune encephalomyelitis. Brain, Behavior and Immunity, 122, 202–215. https://doi.org/10.1016/j.bbi.2024.08.023

Brain, Behavior, and Immunity 122 (2024) 202–215

Contents lists available at ScienceDirect

Brain Behavior and Immunity

journal homepage: www.elsevier.com/locate/ybrbi

Retigabine, a potassium channel opener, restores thalamocortical neuron functionality in a murine model of autoimmune encephalomyelitis

Luca Fazio [a,*,1], Venu Narayanan Naik [b,1], Rajeevan Narayanan Therpurakal [a], Fiorella M. Gomez Osorio [a], Nicole Rychlik [c], Julia Ladewig [d,e,f], Michael Strüber [g], Manuela Cerina [b], Sven G. Meuth [a,2], Thomas Budde [c,*,2]

[a] Department of Neurology, University of Düsseldorf, Düsseldorf, Germany
[b] Department of Neurology with Institute of Translational Neurology, University Hospital Münster, Münster, Germany
[c] Institute of Physiology I, University of Münster, Münster, Germany
[d] Department of Translational Brain Research, Central Institute of Mental Health (ZI), University of Heidelberg/Medical Faculty Mannheim, Germany
[e] HITBR Hector Institute for Translational Brain Research gGmbH, Mannheim, Germany
[f] German Cancer Research Center (DKFZ), Heidelberg, Germany
[g] Epilepsy Center Frankfurt Rhine-Main, Center of Neurology and Neurosurgery, Goethe University, Frankfurt, Germany

ARTICLE INFO

Keywords:
Retigabine
Cytokines
Inflammation
Thalamus
Multiple sclerosis
KCNQ

ABSTRACT

Background: Multiple Sclerosis (MS) is an autoimmune neurodegenerative disease, whose primary hallmark is the occurrence of inflammatory lesions in white and grey matter structures. Increasing evidence in MS patients and respective murine models reported an impaired ionic homeostasis driven by inflammatory-demyelination, thereby profoundly affecting signal propagation. However, the impact of a focal inflammatory lesion on single-cell and network functionality has hitherto not been fully elucidated.

Objectives: In this study, we sought to determine the consequences of a localized cortical inflammatory lesion on the excitability and firing pattern of thalamic neurons in the auditory system. Moreover, we tested the neuroprotective effect of Retigabine (RTG), a specific K_v7 channel opener, on disease outcome.

Methods: To resemble the human disease, we focally administered pro-inflammatory cytokines, TNF-α and IFN-γ, in the primary auditory cortex (A1) of MOG_{35-55} immunized mice. Thereafter, we investigated the impact of the induced inflammatory milieu on afferent thalamocortical (TC) neurons, by performing *ex vivo* recordings. Moreover, we explored the effect of K_v7 channel modulation with RTG on auditory information processing, using *in vivo* electrophysiological approaches.

Results: Our results revealed that a cortical inflammatory lesion profoundly affected the excitability and firing pattern of neighboring TC neurons. Noteworthy, RTG restored control-like values and TC tonotopic mapping.

Conclusion: Our results suggest that RTG treatment might robustly mitigate inflammation-induced altered excitability and preserve ascending information processing.

Abbreviations: A1, Primary auditory cortex; AP, Action potential; ACSF, Artificial-cerebrospinal fluid; BBB, Blood-brain-barrier; Ca^{2+}, Calcium; CNS, Central nervous system; DAPI, 4′,6-diamidino-2-phenylindole, dihydrochloride; DPI, Days post immunization; EAE, Experimental autoimmune encephalomyelitis; GM, Grey matter; IFF, Instantaneous firing frequency; IFN-γ, Interferon gamma; I_M, M−current; ISI, Interspike interval; IVC, Individually ventilated cages; K^+, Potassium; LTS, Low-threshold spike; MGN, Medial geniculate nucleus; MHC, Major histocompatibility complex; MS, Multiple sclerosis; MOG_{35-55}, Myelin oligodendrocyte glycoprotein 35–55; PFA, Paraformaldehyde; PTX, Pertussis Toxin; R_{in}, Input resistance; RMP, Resting membrane potential; RT, Room temperature; RTG, Retigabine; SAL, Saline; SEM, Standard error of the mean; SFA, Spike-frequency accommodation; TC, Thalamocortical; TNF-α, Tumor necrosis factor alpha; vMGN, Ventral medial geniculate nucleus; WT, Wild-type.

* Corresponding authors at: Department of Neurology, University of Düsseldorf, Moorenstraße 5, 40225 Düsseldorf, Germany.
E-mail addresses: Luca.Fazio@med.uni-duesseldorf.de, luca.fazio@hhu.de (L. Fazio), Venu.Narayanannaik@ukmuenster.de (V.N. Naik), Rajeevan.TherpurakalNarayanan@med.uni-duesseldorf.de (R.N. Therpurakal), FiorellaMaria.GomezOsorio@med.uni-duesseldorf.de (F.M. Gomez Osorio), Nicole.Rychlik@ukmuenster.de (N. Rychlik), Julia.Ladewig@zi-mannheim.de (J. Ladewig), strueber@med.uni-frankfurt.de (M. Strüber), SvenGuenther.Meuth@med.uni-duesseldorf.de (S.G. Meuth), tbudde@uni-muenster.de (T. Budde).
[1] Luca Fazio and Venu Narayanan Naik share first authorship.
[2] Sven G. Meuth and Thomas Budde share last authorship.

https://doi.org/10.1016/j.bbi.2024.08.023
Received 30 October 2023; Received in revised form 7 August 2024; Accepted 10 August 2024
Available online 13 August 2024

1. Introduction

Multiple Sclerosis (MS) is a chronic, demyelinating disease of the central nervous system (CNS), characterized by the accumulation of inflammatory lesions in the white- and grey matter of the brain and spinal cord (Filippi et al., 2018). After crossing the blood–brain-barrier (BBB), autoreactive T and B lymphocytes infiltrate into the brain parenchyma, where they secrete soluble mediators, such as pro-inflammatory cytokines, promoting gliosis and a gradual neurodegeneration, which correlates with clinical disability (Goverman, 2009). Noteworthy, inflammatory demyelination may be observed in several cortical and deep grey matter areas, including the thalamus, from the earliest stages of the disease (Calabrese et al., 2009; Geurts, 2012), thereby suggesting a paramount role played by an altered functionality of the TC system at the basis of MS pathogenesis (Crandall et al., 2015; Groh et al., 2014; Suga, 2012).

Except for the olfactory pathway, all sensory inputs are filtered and processed in the thalamus. Notably, the medial geniculate nucleus (MGN) of the auditory thalamus is endowed with tonotopically organized TC neurons, conveying and shaping incoming stimuli to the primary auditory cortex (A1) by means of two peculiar firing modes, defined as tonic and burst activity (Sherman, 2001; Iavarone et al., 2019). Tonic firing is characterized by a regular pattern of action potentials (APs), encoding and relaying input from the periphery to the cortex. Conversely, rhythmic bursting is characterized by a brief high-frequency succession of APs, emerging on a low-threshold calcium (Ca^{2+}) spike (LTS), and occurs prominently during physiological sleep or specific neurological disorders (Wang et al., 2020; Murray and Anticevic, 2017; Groh et al., 2018).

Functional abnormalities, reshaping in neuronal morphology and silent microstructural alterations in TC circuitry were suggested to be putative underlying mechanisms in the pathogenesis of fatigue and cognitive impairment in MS patients (Deppe et al., 2016; Capone et al., 2020; Rojas et al., 2018; Evangelou et al., 2001). Further electrophysiological investigations revealed a profound impact of myelin loss and regrowth on neuronal excitability and signal propagation (Cerina et al., 2017; Ghaffarian et al., 2016), thereby indicating alterations in the distribution and expression of specific ion channels as a pathological hallmark of the disease (Bittner et al., 2013; Meuth et al., 2008; Jukkola et al., 2012; Bouafia et al., 2014). Previously, we demonstrated that dynamic changes in network and single-cell intrinsic excitability, accompanied by remodeling of the tonotopic organization of the auditory pathway (Cerina et al., 2017), emerged as a result of an aberrant neuron-oligodendrocyte potassium (K^+) shuttling and homeostasis upon inflammatory demyelination (Kapell et al., 2023). Notably, neuronal K_v7 ($K_v7.2$-$K_v7.5$) channels are robustly expressed in central, peripheral and sensory neurons (Trimmer, 2015). Here, opening of these channels mediates an outward hyperpolarizing current, termed M−current (I_M), exerting a pivotal role in regulating neuronal excitability and shaping AP discharge (Baculis et al., 2020). Neuronal K_v7 primarily assemble into $K_v7.2$–7.3 heterotetramers, and their activity can be pharmacologically modulated by the small molecule retigabine (RTG). By means of electrophysiological and behavioral studies, we further demonstrated the neuroprotective potential of RTG treatment on disease outcome, thereby indicating that such approach may potentially counteract MS-driven neurodegeneration (Kapell et al., 2023).

However, the underlying mechanisms through which inflammatory mediators characterizing grey matter lesions ultimately promote neurodegeneration require further investigations and animal models specifically tailored to address it.

As the TC system seems to have a strategic position in MS pathology and to mimic the occurrence of inflammatory plaques throughout the brain in the human disease, we induced a grey matter lesion in the A1 of MOG_{35-55} immunized animals, by means of focal administration of tumor necrosis factor alpha (TNF-α) and interferon gamma (IFN-γ). Then, we assessed the effect of focal experimental autoimmune encephalomyelitis (EAE) induction on TC cell excitability and firing pattern, by performing *ex vivo* electrophysiological single-cell recordings. Moreover, we investigated the functionality of the auditory TC network, by means of *in vivo* longitudinal recordings over the course of EAE and tested the neuroprotective effect of RTG. Further, we explored the relative contribution of different K_v7 isoforms, by characterizing single-cell channel activity and network excitability in *Kcnq3* deficient mice.

2. Materials and methods

2.1. Animals

All animal experiments were approved by the responsible local authority (Landesamt für Natur, Umwelt und Verbraucherschutz Nordrhein-Westfalen; approval ID: 84-02.04.2015.A585 and 81-02.04.2018.A266) and performed in compliance with the ARRIVE guidelines and the 2010/63/EU of the European Parliament and of the Council of 22 September 2010. Animals were kept in groups in individually ventilated cages (IVC) and maintained on a 12-hour light/dark cycle, with food and water available *ad libitum*. Constitutive *Kcnq3* knock-out (*Kcnq3*$^{-/-}$) mice were obtained from Thomas J. Jentsch (Charité – University Medicine, Berlin) and had been generated as previously described (Gao et al., 2021). C57BL/6J mice were used as controls (termed wild-type, WT, hereinafter).

2.2. EAE induction and clinical scoring

Active EAE was induced in female WT (Jackson Lab) and *Kcnq3*$^{-/-}$ mice at 8–14 weeks of age. Animals were immunized by subcutaneous injection of 200 µg MOG_{35-55} peptide (Charité – University Medicine, Berlin) and 5 mg/ml of non-viable *Mycobacterium tuberculosis* H37RA extract (Difco) emulsified in complete Freund's adjuvant (200 µl per mouse; Sigma-Aldrich). On the day of immunization (day 0) and 48 h later (day 2), 400 ng *Bordetella pertussis toxin* (PTX, Enzo Life Sciences) were administered intraperitoneally. Disease severity was evaluated daily using a 10-point scoring system, as previously described (Kapell et al., 2023).

2.3. Surgery − focal injection of cytokines

Cytokine injections in the primary auditory cortex (A1) were performed ten days following EAE induction. Mice were deeply anesthetized and thereafter placed in a stereotactic frame, as previously described (Narayanan et al., 2018). The scalp above the dorsal cortex was excised and the skull was exposed. The following coordinates were measured to target A1: anteroposterior, −2.18 mm; lateral, +4.2 mm relative to Bregma; dorsoventral, 1 mm from the brain surface (Keith and Franklin, 2019). Craniotomies were performed unilaterally (left hemisphere) above the target area using a dental drill and 1 µl of a solution filled with 150 U/mg TNF-α and 800 U/mg IFN-γ dissolved in PBS was injected in layer IV of A1 (200 nl/min). EAE mice receiving a stereotactic injection of PBS in the same region served as controls. Following surgery, the skin was sutured and animals were allowed to recover for 30 min on a warm pad prior to returning to their home cages.

2.4. Tissue preparation for histology and IHC

Mice were transcardially perfused with phosphate buffer saline (PBS) and paraformaldehyde (PFA). Thereafter, tissues were postfixed for 24 h in 4 % PFA prior to being transferred to PBS. Serial coronal brain slices (75 µm thickness) containing the auditory TC system were prepared on a vibratome (7000smz-2, Campden Instruments).

2.5. Conventional IHC

For inflammatory markers, sections were washed in PBS and thereafter blocked with a filtered solution containing 0.25 % Triton X-100 and 5 % normal goat serum (Abcam) in PBS for 90 min at room temperature (RT). Primary antibody incubations were carried out overnight at 4 °C with rabbit anti-Iba1 (1:500, Fujifilm Wako Pure Chemical Corporation) and mouse anti-rat major histocompatibility complex (MHC) Class I RT1A OX-18 (1:100, Bio-Rad). For secondary antibody reaction, slices were incubated for 2 h at RT in a solution containing 1:500 anti-rabbit IgG (H+L) Alexa Fluor 488 conjugate (ThermoFisher Scientific), 1:500 goat anti-mouse IgG (H+L) Cy3 (Sigma-Aldrich), and 1:1000 DAPI (4′,6-diamidino-2-phenylindole, dihydrochloride, Invitrogen). Subsequently, tissues were mounted on glass slides using SlowFade Gold (Invitrogen).

2.6. Tissue preparation for patch-clamp recordings

Animals were sacrificed under deep isoflurane (4 % in O_2, CP-Pharma) anesthesia and brain tissue was gently removed from the skull. Acute brain slices (250 μm) containing the ventral medial geniculate nucleus (vMGN) of the thalamus were prepared as coronal sections on a vibratome (Leica) in ice-cold (< 4 °C) oxygenated slicing solution composed of (in mM): KCl, 2.5; NaH_2PO_4, 1.25; $MgSO_4$, 10; PIPES, 20; Glucose, 10; Saccharose, 200; $CaCl_2$, 0.5 (Merck); pH 7.5. Hereafter, slices were incubated for 30 min in a holding chamber filled with warm (32 °C) artificial cerebro-spinal fluid (ACSF) containing (in mM): NaCl, 1.25; $NaHCO_3$, 24; NaH_2PO_4, 12.5; KCl, 25; Glucose, 10; $CaCl_2$, 2; $MgSO_4$, 2; pH 7.35. Before recording, slices were allowed to recover at RT (23 °C) for 1 h.

2.7. Whole-cell patch-clamp recordings

Whole-cell recordings were carried out in a submerged chamber constantly perfused at 2 ml/min with carbogenated ACSF composed of (in mM): NaCl, 120; KCl, 2.5; NaH_2PO_4, 1.25; $NaHCO_3$, 22; glucose, 25; $CaCl_2$, 2; $MgSO_4$, 2; pH 7.35. Recordings were performed on the soma of visually identified vMGN TC neurons using patch pipettes pulled from borosilicate glass capillaries (Harvard Apparatus) filled with a K^+-gluconate-based solution containing (in mM): NaCl, 10; K^+-gluconate, 88; K_3-citrate, 20; HEPES, 10; BAPTA, 3; Phosphocreatine, 15; $MgCl_2$, 1; $CaCl_2$, 0.5; Mg-ATP, 3; Na-GTP, 0.5; pH 7.25; 295 mOsmol/kg. Typical electrode resistance was 5–6 MΩ, with a series resistance in the range of 5–15 MΩ (compensation ≥ 20 %). Electrodes were connected to an EPC10 amplifier (Heka Elektronik) and electrical activity was measured using the software PatchMaster (HEKA Elektronik). Recordings were corrected offline for liquid junction potential. Current-clamp measurements were performed in standard ACSF, whereas voltage-clamp recordings were carried out in a solution containing (in μM): mibefradil, 2; nifedipine, 1; ZD7288, 30; tetrodotoxin (TTX), 0.5 (see Supplementary Methods). Electrophysiological *ex vivo* recordings were performed in the perilesional and contralateral hemisphere of cytokine-injected mice (hereinafter termed EAE ipsi and EAE contra, respectively), in EAE mice received an intracortical injection of PBS (EAE PBS), whilst WT mice without focal EAE induction served as additional controls.

2.8. Morphological identification of recorded TC neurons

During recording, neurons were passively filled with 0.5 % biocytin (Sigma Aldrich) and thereafter brain slices were fixed in 4 % PFA overnight for subsequent post hoc visualization. After being washed in PBS, slices were incubated in a blocking solution containing 1 % Triton X-100 and 2 % bovine serum albumin in PBS for 1 h at RT and subsequently processed for immunostaining with 5 μg/ml Streptavidin Cy3 conjugate (Sigma S-6402) for 3 h at RT. Tissues were washed five times in PBS and mounted on glass slides using SlowFade Gold (Invitrogen).

2.9. Image acquisition

Images were acquired using a fluorescence microscope (Keyence, BZ-X800) equipped with 4x and 20x Plan Apochromat objectives. Whole hemisphere streptavidin staining tiled images were taken with a 4x objective and processed using Keyence BZ-X800 Analyzer Software version 1.1.2.4. Z-stack images of Iba1-positive cells were acquired with a 40x Plan Apochromat objective and converted into maximum projection images using the full focus sectioning feature of the BZ-X800 Analyzer.

2.10. Electrode implantation

For electrode implantation, ten days prior to EAE induction animals were anaesthetized and placed in a stereotactic apparatus as previously described (see Surgery – focal injection of cytokines). Craniotomies were performed unilaterally (left hemisphere) to accommodate microwire arrays (one array, eight electrodes and one reference/array per brain region; Stablohm 650; California Fine Wire) in the vMGN, as previously reported (Narayanan et al., 2018). Thereafter, mice recovered on a heating pad for 30 min before being housed in IVC racks. Following surgery, the health status of the animals and their recovery were monitored daily for ten days prior to experimentation.

2.11. In vivo electrophysiological recordings

WT and *Kcnq3*$^{-/-}$ mice were allowed to recover for ten days following electrode implantation prior to be MOG_{35-55} immunized. Starting from the day of EAE induction (day 0), WT animals received daily an intraperitoneal injection of either RTG (1 mg/kg) or saline (SAL) and unitary activity recordings were performed during the early (day 12) and chronic (day 35) stage of the disease. Recordings carried out prior to immunization served as a control. The impact of *Kcnq3* deletion on neuronal activity was assessed by performing recordings at the same time points in untreated WT and *Kcnq3*$^{-/-}$ animals. To determine frequency-related responses of thalamic neurons of the vMGN, recordings were performed in freely moving mice before and during the presentation of an auditory stimulus consisting of six repetitions of either low- or high-frequency tones (2.5 kHz and 10 kHz at 85 dB, respectively), as previously described (Narayanan et al., 2018; Daldrup, 2016) (Supplementary Methods).

2.12. Statistical analysis

All results are presented in the text as mean ± SEM. Statistical significance of data with a Gaussian distribution was determined using unpaired two-tailed Student's *t*-test. Statistical comparisons across three or more groups were performed using one-way ANOVA or factorial mixed design ANOVAs, followed by Tukey, Dunnett or Šidák post-hoc test. Multiple comparisons were assessed by two-way ANOVA or factorial mixed design ANOVA, complemented by Tukey post-hoc test. Statistical significance differences were reported using the following p-values: $p < 0.05$ (*), $p < 0.01$ (**), $p < 0.001$ (***), and $p < 0.0001$ (****). GraphPad Prism (version 9.3.1), Origin, and Adobe Illustrator were used for data analysis and figure preparation.

3. Results

3.1. Immunofluorescence staining reveals dense infiltrates of activated microglia in A1 upon focal cytokine injection

A hallmark of MS is the occurrence of cortical inflammatory lesions, profoundly affecting clinical manifestations and disease progression. To mimic the human pathology and assess the impact of a focal targeted grey matter lesion on TC neuron functionality, 10 days post

immunization (dpi), we stereotactically injected TNF-α and IFN-γ into the left A1 of EAE mice (Fig. 1), whilst animals receiving a focal injection of PBS served as controls. First, in order to verify the presence of inflammatory lesions in our model, we immunohistochemically visualized microglia and we explored their activation status using the MHC class I antigen (OX-18) in the perilesional hemisphere of cytokine- and PBS-injected mice. Dense infiltrates of activated microglia were detected in the ipsilateral auditory cortex upon cytokine injection at 12 dpi (Fig. 2A) and persisted in chronic EAE (Fig. 2C). Conversely, the perilesional area of mice which received an intracortical injection of PBS was characterized by less microglia activation, confined to the proximity of the needle track (Fig. 2B, D). Noteworthy, microglia displayed enlarged and more irregular cell bodies upon focal cytokine injection (Fig. 2A'), in comparison to PBS (Fig. 2B'), accompanied by colocalization of Iba1 and OX-18, thereby suggesting a persisting and more robust microglia activation following focal cytokine injection (Fig. 2C'), in comparison to PBS (Fig. 2D'). Immunofluorescence staining in the contralateral hemisphere of cytokine-injected mice revealed the higher specificity of inflammatory lesions and microglia activation driven by the injection of inflammatory mediators in A1 (Fig. S1).

3.2. TC neuron excitability is modulated by focal injection of cytokines in A1

To determine the impact of focal EAE induction on neuronal excitability, we characterized vMGN TC neuron activity *ex vivo* in acute brain slices, by performing whole-cell current-clamp recordings in the hemisphere where the cytokines were injected (ipsilateral hemisphere), 12 and 35 days after EAE induction (Fig. 1). Recordings carried out in PBS-injected mice and naïve WT without focal EAE induction served as controls. Tonic firing was evoked by injecting direct current steps of increasing amplitude (from +20 pA to +160 pA, 20 pA increment), while holding the cell at −55 mV (Fig. 3A). Recordings performed in the ipsilateral hemisphere revealed the emergence of a hyperexcitable phenotype of TC neurons at 12 dpi, as compared to cells recorded in WT (+160 pA, $p = 0.0006$), thereby indicating that focal injection of cytokines in the A1 profoundly affects the degree of excitability of thalamic relay cells (Fig. 3 A'). Further, to explore dynamic changes in TC neuron activity as the disease converts to a neurodegenerative stage, we performed electrophysiological recordings at 35 dpi (Fig. 3B). Interestingly, a robust increase in the number of APs was observed in neurons recorded in the ipsilateral hemisphere compared to both PBS (+160 pA, $p = 0.0002$) and WT animals (+160 pA, $p < 0.0001$) (Fig. 3 B').

Next, we investigated temporal aspects of stimulus-evoked TC neuron activity by plotting the instantaneous firing frequency (IFF) of consecutive APs vs. the interspike interval (ISI) number. The firing pattern of TC neurons recorded in the ipsilateral hemisphere at 12 dpi was characterized by a significantly increased initial IFF, in comparison to both TC neurons in the PBS-injected hemisphere ($p < 0.0001$) and WT ($p = 0.0009$) (Fig. 3C). The initial AP discharge was followed by a post-burst accommodation, characterized by a progressively increasing ISI in all experimental groups. The same experimental approach was employed to monitor dynamic changes in the firing pattern and frequency of AP discharge in the neurodegenerative stage of the EAE course (35 dpi). However, no significant differences were observed between TC neurons recorded from the ipsilateral hemisphere of EAE animals and both PBS and WT controls (Fig. 3D). Morphological and histological features of vMGN TC neurons were identified by inclusion of biocytin in the recording pipette and subsequent streptavidin staining (Fig. 3E). Neurons with typical characteristics were identified revealing large cell bodies (15–25 μm in diameter) giving rise to three to six dendrites (Kanyshkova et al., 2012; Budde et al., 2023).

Taken together, these results suggest that pro-inflammatory cytokines, such as TNF-α and IFN-γ, play a paramount role in driving hyperexcitability of TC relay neurons of the vMGN, thereby highlighting the modulation of thalamic components of the TC system both at the preclinical and progressive neurodegenerative phase of the disease course.

3.3. Pro-inflammatory cytokines drive enhancement of LTS-mediated firing in vMGN neurons

To explore the effect of pro-inflammatory mediators on LTS generation in TC neurons, we challenged vMGN neurons with depolarizing

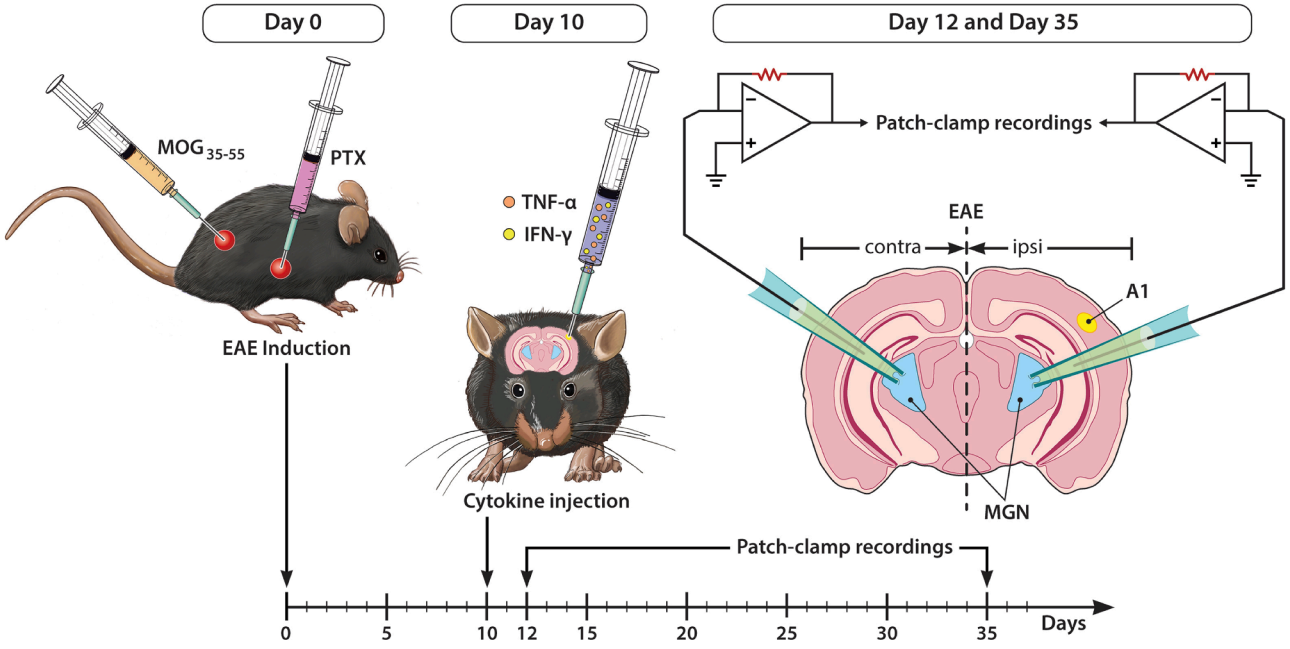

Fig. 1. Graphic representation of the *ex-vivo* experimental design. WT and *Kcnq3*$^{(-/-)}$ mice were administered myelin oligodendrocyte glycoprotein (MOG_{35-55}) and *Micobacterium tuberculosis* emulsified in complete Freund's adjuvant, and treated with *Bordetella pertussis toxin* (PTX) (day 0). A focal EAE was induced in WT mice at day 10, by injecting the proinflammatory cytokines TNF-α and IFN-γ into the left A1 (EAE ipsi). Electrophysiological *ex-vivo* recordings were performed in the vMGN of the thalamus in the early (day 12) and chronic (day 35) phase of the EAE course.

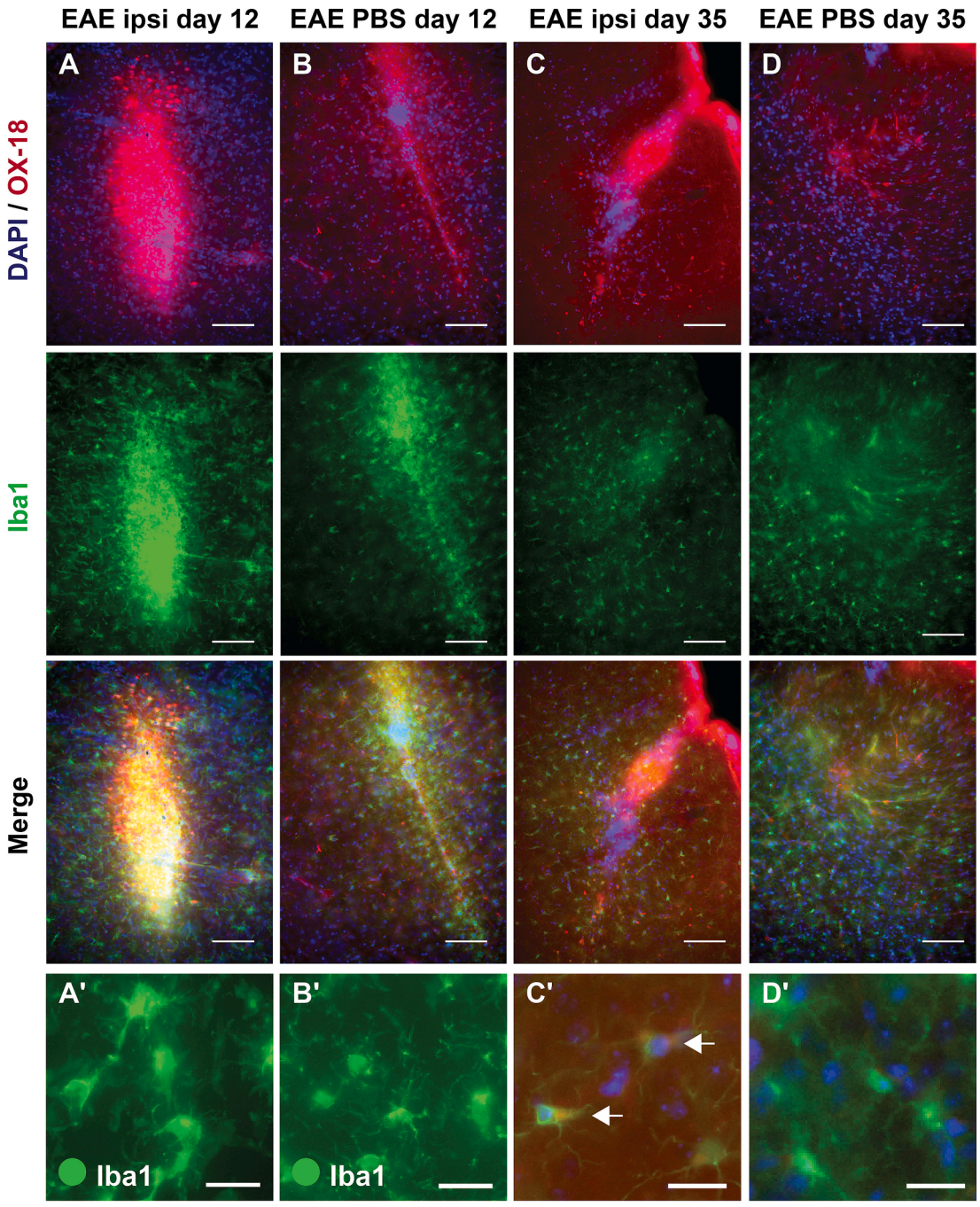

Fig. 2. Immunofluorescence staining reveals dense infiltrates of activated microglia upon focal cytokine injection. Representative photomicrographs and close-ups of the ipsilateral auditory cortex of cytokine- and PBS-injected EAE mice immunostained with DAPI (nuclear marker), OX-18 (MHC class I antigen), and Iba1 (microglia marker), in the acute (day 12) and chronic stage (day 35) of the EAE course. The perilesional area of cytokine-injected mice is characterized by a higher infiltration of activated microglia 12 (**A, B**) and 35 dpi (**C, D**), as compared to animals which received a PBS injection. Scale bars: 500 μm. Close-ups of the Iba1-positive cell morphology revealing an enlarged and more irregular soma upon focal cytokine injection (**A'**), in comparison to PBS (**B'**). Colocalization of Iba1 (green) and OX-18 (red) was observed in the perilesional cytokine-injected area (**C'**, indicated by arrows), but not in PBS (**D'**). Scale bars: 20 μm.

and hyperpolarizing current pulses (+160 pA and −180pA, respectively) from resting membrane potential (RMP) and analyzed the number of LTS-mediated APs. In response to a depolarizing current pulse, the number of LTS-mediated APs was not significantly increased upon EAE induction at 12 dpi (Fig. 4A, A'). However, in the chronic stage of the disease (Fig. 3B, B'), we observed a higher number of LTS-APs at the onset of the depolarizing current input, thereby indicating that cytokine injection facilitated the emergence of burst firing in TC neurons recorded from the ipsilateral vMGN, as compared to WT controls ($p = 0.0446$).

Next, we stimulated TC neurons with a hyperpolarizing current injection and measured the number of LTS-mediated spikes characterizing rebound bursts (Fig. 3 C, D). Accordingly, TC neurons displayed a tendency to fire a larger number of APs 12 and 35 days following EAE induction, although without reaching significance threshold (Fig. C', D').

Collectively, these findings suggest that intrinsic hyperexcitability driven by inflammatory mediators is accompanied by dynamic changes in the firing pattern of TC neurons, thereby facilitating the emergence of bursting activity following a focal inflammatory lesion in the A1. Noteworthy, no significant differences emerged when single-cell

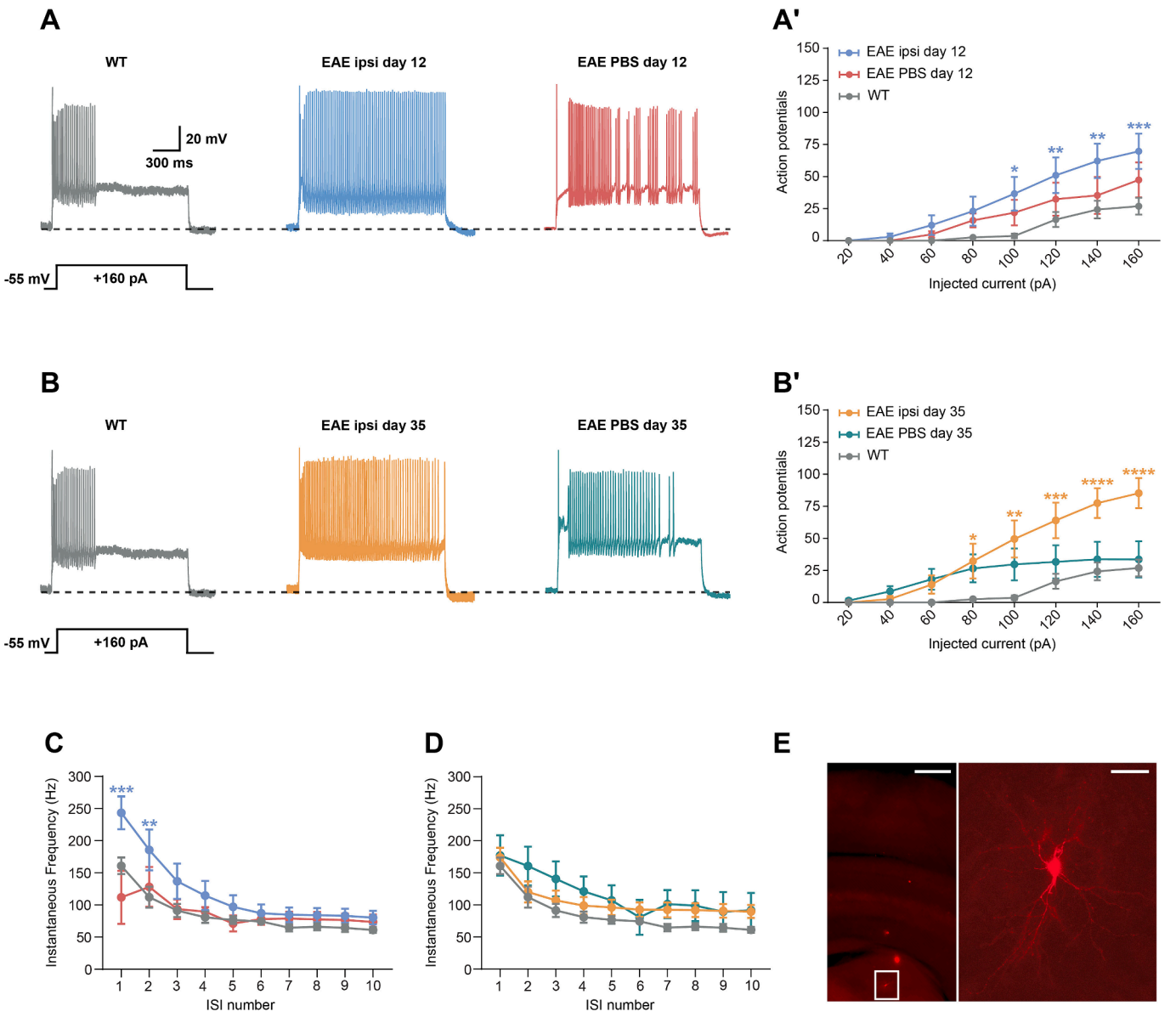

Fig. 3. TC neuron excitability is modulated by focal injection of cytokines in A1. (**A**, **B**) Representative voltage responses from vMGN TC cells to +160 pA current input. Recordings were performed in WT (gray), EAE ipsi (day 12, blue; day 35, orange), and EAE PBS (day 12, red; day 35, green) mice. (**A'**) Number of APs elicited in WT and EAE mice upon current injections of 20–160 pA, measured at day 12 (n = 7 cells from 3 wt mice; EAE ipsi day 12 = 7 cells from 5 mice; EAE PBS day 12 = 6 cells from 3 animals; WT vs. EAE ipsi day 12, + 100 pA, p = 0.014; +120 pA, p = 0.0069; +140 pA, p = 0.0026; +160 pA, p = 0.0006, two-way ANOVA complemented by Tukey's test for multiple comparison). (**B'**) Number of APs evoked at day 35 of the EAE course (n = 7 cells from 3 wt mice; EAE ipsi day 35 = 7 cells from 4 animals; EAE PBS day 35 = 7 cells from 3 animals; WT vs. EAE ipsi day 35, +80 pA, p = 0.0424; +100 pA, p = 0.0011; +120 pA, p = 0.0004; +140 pA, p < 0.0001; +160 pA, p < 0.0001; EAE ipsi day 35 vs. EAE PBS day 35, +120 pA, p = 0.0302; +140 pA, p = 0.0019; +160 pA, p = 0.0002, two-way ANOVA complemented by Tukey's test for multiple comparison). (**C**) IFF according to the relative ISI measured in WT and EAE mice 12 dpi (n = 7 cells from 3 wt mice; EAE ipsi day 12 = 7 cells from 5 mice; EAE PBS day 12 = 5 cells from 3 animals; WT vs EAE ipsi day 12, ISI #1, p = 0.0009; ISI #2, p = 0.0036; EAE ipsi day 12 vs EAE PBS day 12, ISI #1, p < 0.0001, two-way ANOVA complemented by Tukey's test for multiple comparison). (**D**) IFF/ISI relationship measured 35 dpi (n = 7 cells from 3 wt mice; EAE ipsi day 35 = 7 cells from 4 animals; EAE PBS day 35 = 6 cells from 3 animals). (**E**) Z-projection image of a representative TC neuron filled with biocytin and thereafter stained with streptavidin. Left, low magnification image of the soma-containing coronal section. Scale bar: 500 μm. Right, maximum projection of the stained TC neuron. Scale bar: 50 μm. Error bars represented as mean ± SEM; $p < 0.05$ (*), $p < 0.01$ (**), $p < 0.001$ (***), $p < 0.0001$ (****). See also Supplementary statistical analysis.

excitability and the firing pattern of neurons recorded in PBS animals and in the contralateral hemisphere of cytokine-injected mice were compared (Fig. S2).

3.4. Effect of Kcnq3 deletion on firing pattern and intrinsic properties of vMGN TC neurons

RTG is a selective $K_v7.2$–7.5 channel agonist, exerting its action by potentiating I_M generation and, consequently, robustly attenuating inflammation-induced hyperactivity of TC neurons (Fig. S3). In the following, we characterized the impact of $K_v7.3$ subunits on intrinsic excitability and mediating the RTG effect, by performing *ex vivo* patch-clamp recordings in acute brain slices from *Kcnq3* deficient mice (Fig. 5A). First, we explored differences in active membrane properties between genotypes by examining TC neuron excitability, using a series of increasing depolarizing current pulses (20–160 pA, 1.5 s duration).

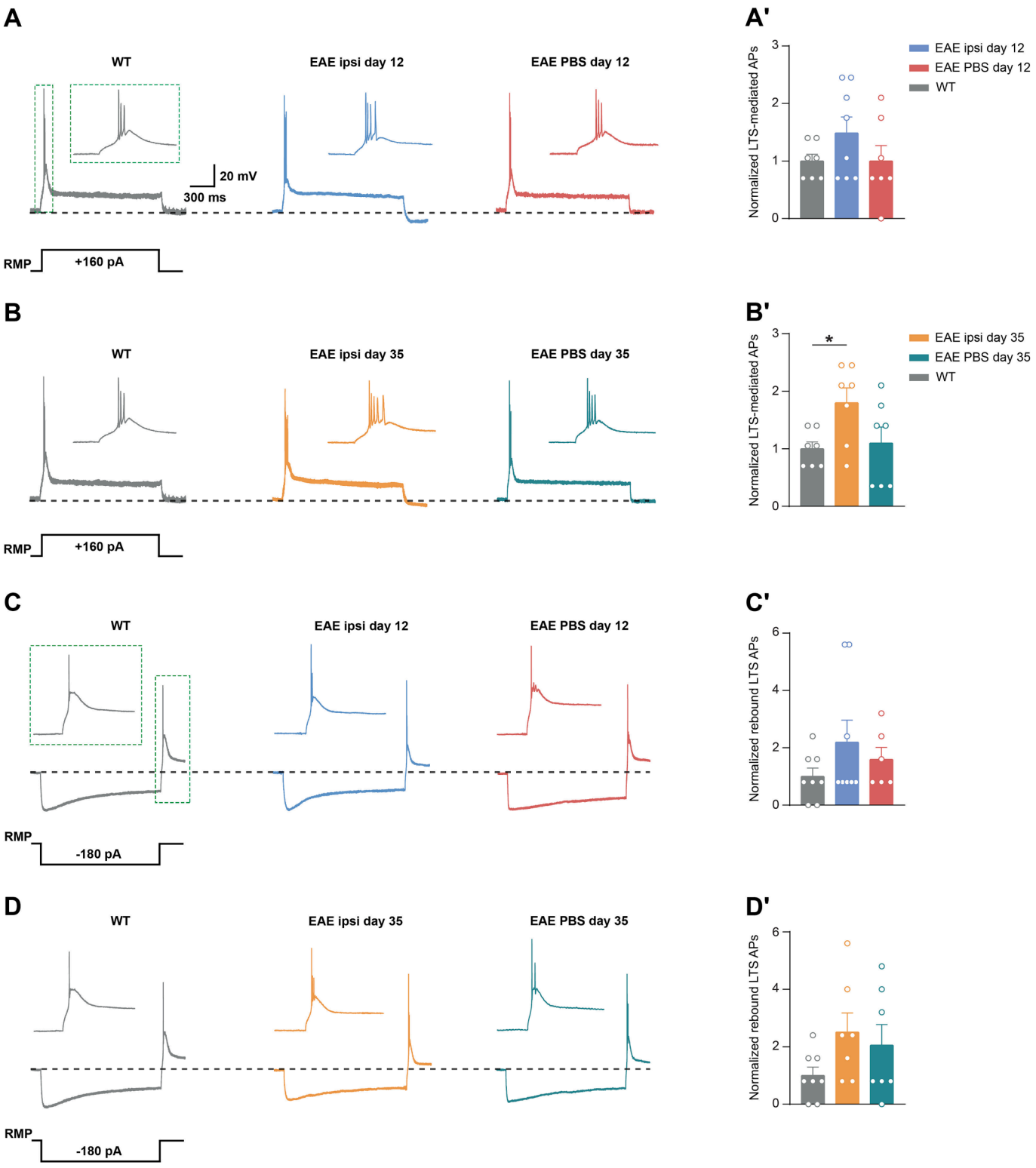

Fig. 4. Proinflammatory mediators drive enhancement of burst firing in vMGN neurons. Induction of an inflammatory lesion in A1 facilitated TC burst firing in the perilesional vMGN in chronic EAE. Recordings were carried out in WT (gray), EAE ipsi (day 12, blue; day 35, orange), and EAE PBS (day 12, red; day 35, green) animals. (**A**, **B**) Exemplary vMGN TC current-clamp traces evoked in response to a + 160 pA input from RMP. (**A'**, **B'**) Normalized number of LTS-mediated APs elicited in WT and EAE animals in the acute (**A'**) and chronic (**B'**) stage of the EAE course (n = 7 cells from 3 wt mice; EAE ipsi day 12 = 8 cells from 5 mice; EAE PBS day 12 = 7 cells from 3 animals; EAE ipsi day 35 = 7 cells from 4 animals; EAE PBS day 35 = 7 cells from 3 animals; WT vs. EAE ipsi day 35, p = 0.0446, one-way ANOVA complemented by Dunnett test for multiple comparison). (**C**, **D**) Sample traces displaying rebound burst firing of TC neurons elicited following application of a hyperpolarizing current pulse (−180 pA, 1.5 s duration). (**C'**, **D'**). Number of rebound LTS-triggered APs induced by a hyperpolarizing pulse, 12 (**C'**) and 35 (**D'**) days following EAE induction (n = 8 cells from 3 wt mice; EAE ipsi day 12 = 8 cells from 5 mice; EAE PBS day 12 = 6 cells from 3 animals; EAE ipsi day 35 = 7 cells from 4 animals; EAE PBS day 35 = 7 cells from 3 animals). Error bars represented as mean ± SEM; $p < 0.05$ (*). See also Supplementary statistical analysis.

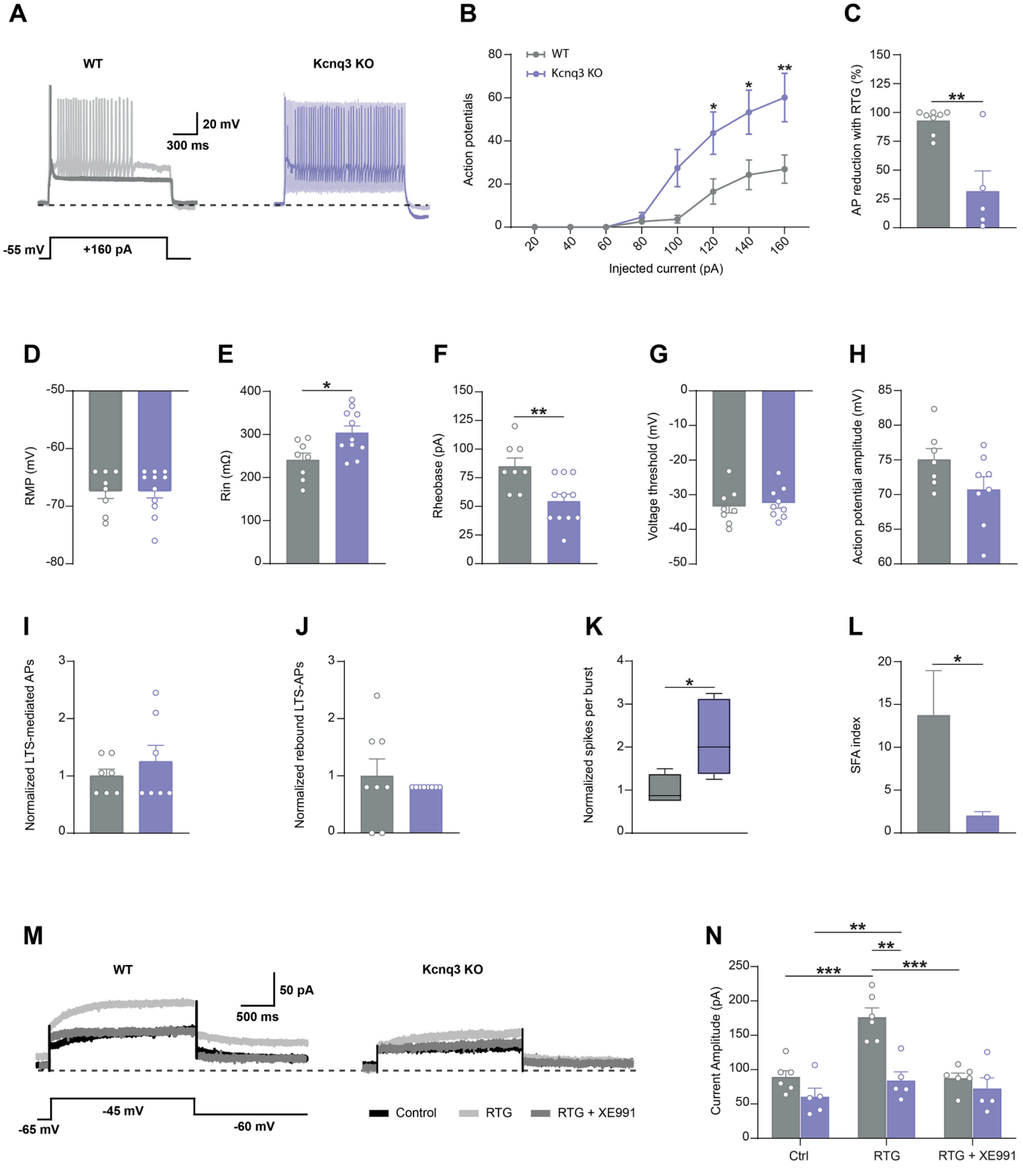

(caption on next page)

Fig. 5. Effect of *Kcnq3* deletion on firing pattern and intrinsic properties of vMGN TC neurons. (**A**) Exemplary voltage responses of TC neurons to a depolarizing (+160 pA) current pulse in WT (gray) and *Kcnq3*$^{(-/-)}$ (purple) mice, recorded under control conditions (shaded traces) and in the presence of RTG. (**B**) Number of APs evoked in response to the injection of positive currents with 20 pA increments from RMP. *Kcnq3* deletion promoted a significantly increased excitability of TC neurons (n = 8 cells from 3 wt mice; *Kcnq3*$^{(-/-)}$ = 10 cells from 5 mice; +120 pA, p = 0.0224; +140 pA, p = 0.0112; + 160 pA, p = 0.0023, two-way ANOVA complemented by Šidák's test for multiple comparison). (**C**) Bar graph indicating only a partial percentage AP reduction in *Kcnq3*$^{(-/-)}$ following RTG application in comparison to controls (n = 8 cells from 3 wt mice; *Kcnq3*$^{(-/-)}$ = 5 cells from 3 mice, p = 0.0013, unpaired two-tailed Student's *t*-test). (**D-H**) Comparison of RMP, R_{in} (p = 0.0128, unpaired two-tailed Student's *t*-test), rheobase (p = 0.0051, unpaired two-tailed Student's *t*-test), AP voltage threshold, and AP amplitude. Normalized LTS-mediated and rebound APs elicited in response to depolarizing (**I**) and hyperpolarizing (**J**) current pulses (+160 pA and −180 pA, respectively) from RMP (n = 8 cells from 3 wt mice; *Kcnq3*$^{(-/-)}$ = 5 cells from 3 mice). (**K**) Box plots comparing the normalized number of spikes in each burst. *Kcnq3* loss facilitated the occurrence of a burst discharge characterized by an increased number of spikes as compared to controls (n = 4 cells from 3 wt mice; *Kcnq3*$^{(-/-)}$ = 5 cells from 3 mice, p = 0.040, unpaired two-tailed Student's *t*-test). (**L**) Bar graph indicating a significant increased SFA index in TC neurons recorded from WT animals as compared to *Kcnq3*$^{(-/-)}$ (n = 4 cells from 3 wt mice; *Kcnq3*$^{(-/-)}$ = 5 cells from 3 mice, p = 0.0383, unpaired two-tailed Student's *t*-test). Representative voltage-clamp recordings (**M**) and bar graphs (**N**) indicating the impact of *Kcnq3* deletion on M−current amplitude and the effect of KCNQ channel modulators. *Kcnq3* loss was associated with a significant reduction of the RTG-evoked current in *Kcnq3*$^{(-/-)}$ as compared to WT (n = 7 cells from 3 wt mice; *Kcnq3*$^{(-/-)}$ = 8 cells from 3 mice; WT control vs. WT+RTG, p = 0.0005; *Kcnq3* KO control vs. *Kcnq3* KO+RTG, p = 0.0076, mixed model two-way ANOVA complemented by Tukey's test for multiple comparison). Error bars represented as mean ± SEM; $p < 0.05$ (*), $p < 0.01$ (**), $p < 0.001$ (***). See also Supplementary statistical analysis.

TC neurons recorded from *Kcnq3* KO mice fired a higher number of APs in response to the same current injection (+160 pA, p = 0.0023) (Fig. 5B). In order to assess the contribution of a specific ion channel modulator in the absence of the K_v7.3 subunits, we further quantified AP reduction in the presence of RTG (Fig. 5C, Fig. S4). Interestingly, RTG application exerted only a partial effect in reducing the number of AP recorded under control conditions in TC neurons from *Kcnq3* KO mice, as compared to WT (p = 0.0013).

Next, we explored differences in the passive properties between genotypes (Fig. 5D-H). No significant differences emerged from the analysis of the RMP. Conversely, TC neurons recorded from mutant mice exhibited a higher input resistance (p = 0.0128) and a lower rheobase (p = 0.0051) compared to WT, thereby strengthening the association between lack of K_v7.3 and thalamic hyperexcitability. Similar voltage threshold and AP amplitude were detected in *Kcnq3* KO and WT mice, thus suggesting a marginal impact of these subunits in shaping AP waveform.

Furthermore, we sought to determine the impact of K_v7.3 on the firing pattern of thalamic cells (Fig. 5I-K). TC neurons from *Kcnq3* KO mice fired bursts consisting of a larger number of spikes (p = 0.040). Moreover, a significantly reduced spike-frequency accommodation (SFA) was observed in mutants (p = 0.0383), thereby suggesting that functional K_v7.3 significantly influence the frequency of AP discharge (Fig. 5L). However, no significant differences were detected in the number of LTS-mediated APs elicited in response to both depolarizing and hyperpolarizing current pulses at RMP. Similarly, temporal aspects of stimulus-evoked TC neuron activity did not differ between WT and mutants (Fig. S4).

The hyperpolarizing I_M in neurons is largely mediated by K_v7.2/7.3 heteromeric channels. Thus, we explored the consequence of K_v7.3 deletion on current generation and in mediating the RTG effect (Fig. 5M, N). Analysis of the average basal K_v7-mediated current revealed only a marginal reduction of I_M amplitude. RTG application led to a significant current increment in both WT (p = 0.0005) and *Kcnq3* KO mice (p = 0.076). However, the agonist-elicited current was much smaller in mutants, as compared to WT (p = 0.0025). Control-like values were restored when RTG and XE991 were simultaneously added to the bath solution.

Collectively, these data clearly indicate that the K_v7.3 subunits strongly influence active and passive membrane properties of TC neurons. Furthermore, RTG-mediated currents largely depend on the presence of functional K_v7.3 channels.

3.5. *Auditory-stimulus discrimination and burst discharge are affected by Kcnq3 loss in vivo*

In order to investigate the impact of *Kcnq3* deletion on neuronal network excitability and sensory information processing driven by inflammation, we performed *in vivo* electrophysiological recordings in vMGN in a longitudinal manner. Here, similarly to previous experimental approaches (Kapell et al., 2023; Narayanan et al., 2018), we presented the mice with two different tones, 2.5 and 10 kHz, and measured changes in stimulus-evoked neuronal activity as compared to baseline in the region representing 10 kHz. Analysis revealed that before EAE induction WT and *Kcnq3* KO animals exhibited a similar response to the not relevant stimulus (2.5 kHz), thereby indicating that *Kcnq3* loss did not influence tone discrimination. However, in line with our previous *ex vivo* findings, an increased firing rate was observed in *Kcnq3* KO mice elicited at 10 kHz (p = 0.021) (Fig. 6A, A'). Twelve days following EAE induction, an increased z-score and stimulus-related firing rates were observed in EAE-*Kcnq3* KO mice irrespectively of the frequency of the presented tone, thereby suggesting a state of neuronal hyperexcitability in response to 2.5 kHz (p < 0.0001) and 10 kHz (p < 0.0005), along with an impaired tonotopic organization of the vMGN (Fig. 6B, B'). Furthermore, we detected an increased baseline activity of thalamic neurons recorded from EAE-*Kcnq3 KO* animals, in the absence of an auditory stimulus (p < 0.0001). Next, we investigated differences in network excitability between EAE-WT and EAE-*Kcnq3 KO* mice by performing *in vivo* recordings in the chronic stage of the disease (35 dpi). Neurons recorded from EAE-*Kcnq3* KO mice were characterized by an increased intrinsic excitability when their baseline activity was assessed, in the absence of an auditory stimulus (p < 0.0008) (Fig. 6C, C'). Strikingly, the stimulus-evoked firing rates did not differ between genotypes, thereby suggesting comparable levels of hyperexcitability at this time point.

We previously showed that *Kcnq3* deletion facilitated the emergence of bursting activity of TC neurons recorded in acute brain slices. Hence, we further explored the consequences of inflammation on high-frequency burst discharges in *Kcnq3* KO mice and respective WT controls. In line with our *ex vivo* electrophysiological investigations, an increased burst firing was detected in *Kcnq3 KO* mice prior to EAE induction (p < 0.0001) (Fig. 6E). This held true when differences in bursting activity between genotypes were assessed at 12 (p = 0.0013) and 35 dpi (p = 0.0111).

Next, we sought to determine whether lack of *Kcnq3* affected the response latency. Prior to EAE induction, response latencies to auditory stimuli were significantly reduced in *Kcnq3 KO* mice, as compared to WT (p = 0.0016) (Fig. 6F). However, no differences between genotypes emerged when response latencies were investigated in the acute (12 dpi) and chronic (35 dpi) stage of the disease.

Collectively, these data indicate that EAE induction is associated with the emergence of hyperexcitability and promotes bursting discharge *in vivo* (Fig. S5A, B). Furthermore, lack of K_v7.3 is associated with an altered auditory network excitability under control conditions and following EAE induction. Facilitation of bursting activity and altered latency responses might indicate a paramount role played by K_v7.3 subunits in ensuring faithful information processing and transmission.

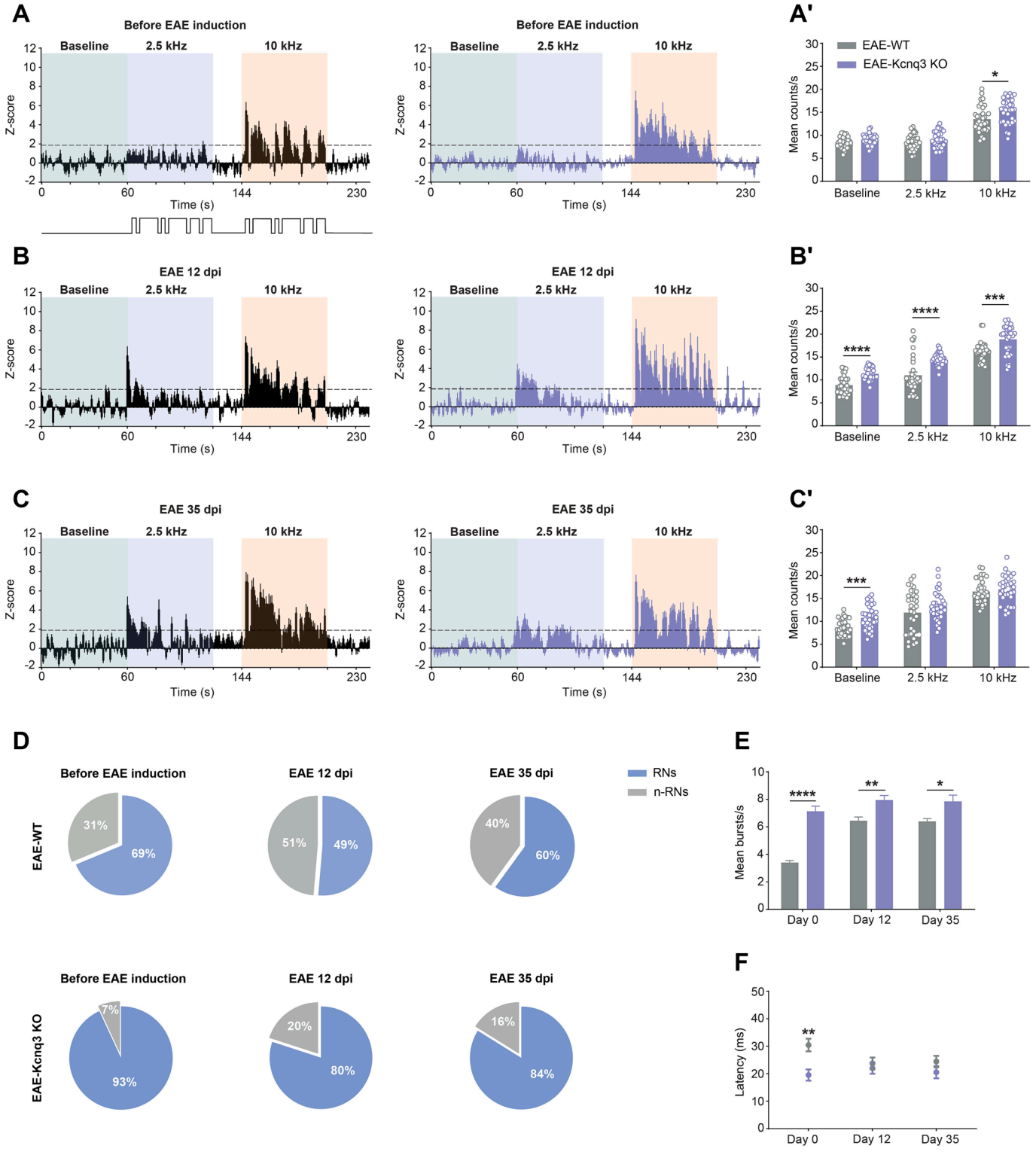

(caption on next page)

Fig. 6. Auditory-stimulus discrimination and burst discharge are affected by Kcnq3 loss *in-vivo*. (**A, B, C**) Z-scores of unitary activity recordings performed during the early (day 12) and chronic (day 35) stage of the disease. Recordings obtained before EAE induction served as a control. Responses of vMGN neurons from WT (black) and *Kcnq3*$^{(-/-)}$ (purple) mice were assessed following the presentation of auditory stimuli of either low (2.5 kHz, blue insets) or high (10 kHz, yellow insets) frequencies. (**A', B', C'**) Bar graphs indicating baseline activity and frequency-specific responsiveness of vMGN neurons. (**A'**) Comparison of the stimulus-evoked neuronal activity (10 kHz) revealed an increased firing rate in mutants (n = 34 cells from 6 wt mice before EAE induction; *Kcnq3*$^{(-/-)}$ = 34 cells from 9 mice before EAE induction; 10 kHz, p = 0.021, two-way ANOVA complemented by Šidák's test for multiple comparison). (**B'**) 12 days following EAE induction TC neurons recorded from *Kcnq3* KO mice displayed an increased firing-rate (n = 34 cells from 6 wt-EAE day 12; EAE-*Kcnq3*$^{(-/-)}$ day 12 = 34 cells from 9 mice; baseline, p < 0.0001; 2.5 kHz, p < 0.0001; 10 kHz, p < 0.0005, two-way ANOVA complemented by Šidák's test for multiple comparison). (**C'**) Thalamic neurons recorded from mutants were characterized by an increased baseline activity 35 days following EAE induction (n = 34 cells from 6 wt-EAE day 35; EAE-*Kcnq3*$^{(-/-)}$ day 35 = 34 cells from 9 mice; baseline, p < 0.0008, two-way ANOVA complemented by Šidák's test for multiple comparison). (**D**) Pie charts representing the percentage of RNs and n-RNs from WT and *Kcnq3*$^{(-/-)}$ mice in the presence of an auditory stimulus. (**E**) Analysis of the firing pattern of vMGN neurons before and after EAE induction revealed that absence of *Kcnq3* facilitated burst discharge (day 0, p < 0.0001; day 12, p = 0.0013; day 35, p = 0.0111, two-way ANOVA complemented by Šidák's test for multiple comparison). (**F**) Bar graphs indicating the latency of vMGN neurons responses following the presentation of an auditory stimulus. Neurons recorded from *Kcnq3*$^{(-/-)}$ animals are characterized by a significantly reduced response latency before EAE induction (p < 0.0001; two-way ANOVA complemented by Šidák's test for multiple comparison). Error bars represented as mean ± SEM; $p < 0.05$ (*), $p < 0.01$ (**), $p < 0.001$ (***), $p < 0.0001$ (****). See also Supplementary statistical analysis.

3.6. RTG treatment reverses the impaired auditory network functionality emerging upon EAE induction

Testing the translational potential of a neuroprotective compound, such as RTG, requires the monitoring of neuronal network dynamics in the living animal over the course of the disease. To address this, single-unit activity was recorded in the vMGN, before and following EAE induction, in freely moving mice treated with either RTG (1 mg/kg) or saline (SAL), by employing the experimental approach described above (Fig. 7). First, we confirmed that the animals were able to discriminate between the two tones (2.5 and 10 kHz) and the absence of intrinsic pre-immunization differences between the two experimental groups by analyzing Z-scores and stimulus-related firing rates in naïve mice (Fig. 7A, A'). Twelve days after immunization, the mice treated with SAL lost their ability to discriminate between the two tones, as reflected by their Z-score increment in response to both 2.5 and 10 kHz (Fig. 7 B). Moreover, the magnitude of the vMGN neuron response was higher as compared to the one observed before immunization. Conversely, treatment with RTG for 12 days following EAE induction indicated a robust reduction in the Z-score in comparison to SAL-treated mice. Analysis of the stimulus-related firing rates at this time point revealed that while the response of the mice treated with RTG did not exceed pre-immunization levels, SAL-treated animals exhibited an increased rate in response to both 2.5 kHz ($p < 0.0001$) and 10 kHz ($p < 0.0001$), thus indicating hyperexcitability (Fig. 6B'). This held true when differences in baseline activity were investigated ($p < 0.0001$). Treatment with RTG significantly reduced thalamic hyperactivity in comparison to SAL-treated mice at baseline ($p < 0.0001$), in response to 2.5 kHz ($p < 0.0001$), and 10 kHz ($p < 0.0001$). Next, we explored the neuroprotective effect of a prophylactic RTG treatment in preventing chronic neuronal hyperexcitability, by measuring single-unit activity 35 dpi (Fig. 6C, C'). Interestingly, similarly to what observed in the acute stage of the disease, we detected a robust reduction in the stimulus-evoked responses to either 2.5 kHz ($p = 0.0160$) and 10 kHz ($p < 0.0001$) in RTG-treated mice as compared to the SAL-control group.

Next, to assess the impact of RTG treatment on TC neuron firing pattern *in vivo*, we measured dynamic changes in burst discharge prior and following EAE induction. In line with our *ex vivo* findings, vMGN neurons exhibited a robust increase in bursting activity upon EAE induction (Fig. 6E). However, RTG treatment resulted in a robust attenuation of burst discharge both 12 ($p < 0.0001$) and 35 dpi ($p < 0.0001$).

No further differences emerged from the analysis of latency responses following auditory stimulation between the two experimental groups (Fig. 6F).

Taken together, our data indicated that RTG treatment reverts immunization-dependent hyperexcitability in our *in vivo* model, thus corroborating the *ex vivo* findings.

4. Discussion

In this study, we aimed to shed light on the contribution of pro-inflammatory mediators to the altered excitability arising upon EAE induction, focusing on the role played by the K_v7 channels and their pharmacological modulation as a neuroprotective strategy to restore neuronal network functionality.

The effect of cytokine release on ion channel function and, thus, neuronal excitability, is an intriguing, but hitherto partially understood component of MS and EAE pathogenesis. Recent studies in the cuprizone model of general de- and remyelination explored changes in the expression and regulation of HCN channel activity driven by inflammatory mediators (Oniani et al., 2022; Chaudhary et al., 2022). Notably, while IFN-α application significantly reduced the number and duration of bursts, presumably by attenuating HCN-mediated currents, an opposite effect was detected in the presence of IL-1β. Divergence and redundancy of pro-inflammatory cytokines, complex signaling cascades, and dynamic changes in their expression throughout the disease, along with intrinsic limitations and variability that experimental models entail, make a translation of such findings into the clinic challenging (Gobel et al., 2018; Bierhansl et a., 2022; Rychlik et al., 2023). In the attempt to mimic the appearance of brain lesions observed in the human disease, here we employed the focal EAE model, by inducing an inflammatory lesion in A1, and investigated its impact on vMGN TC neuron functionality. We found that TC neurons projecting to the hemisphere where the inflammatory lesion was induced (ipsilateral site) exhibited hyperexcitability already at 12 dpi, as compared to recordings performed in both EAE sham and WT control mice. These observations corroborate our recent findings indicating the emergence of a cortical hyperactive phenotype driven by inflammatory demyelination in the acute phase of the disease (Kapell et al., 2023). Our data further suggests that the plethora of inflammatory mediators released by CNS-infiltrated cells, notably TNF-α and IFN-γ, might contribute to the altered excitability observed in MS models. Inflammation-induced maladaptive mechanisms, such as an increased frequency of glutamate-mediated spontaneous and TTX-resistant miniature excitatory postsynaptic currents, were reported to emerge early in the disease and strengthen the link between cytokine release and synaptic dysfunction (Acharjee et al., 2018; Centonze et al., 2009). Accordingly, a recent work by Ellwardt et al. (Ellwardt et al., 2018) hypothesized that cortical hyperactivity in EAE might be mediated by TNF-α secretion. Interestingly, a study by Shim et al. (Shim et al., 2018) revealed that this cytokine promoted an increased excitability of cerebellar neurons by fostering glial glutamate release.

Alongside an increased excitability, we detected an enhanced burst activity in the perilesional vMGN. This firing mode arises as a result of the interplay of specific ionic conductances, such as I_h and I_T (Datunashvili et al., 2018; Cain and Snutch, 2013; Bosch-Bouju et al., 2013) and has been suggested to be a hallmark of pathological

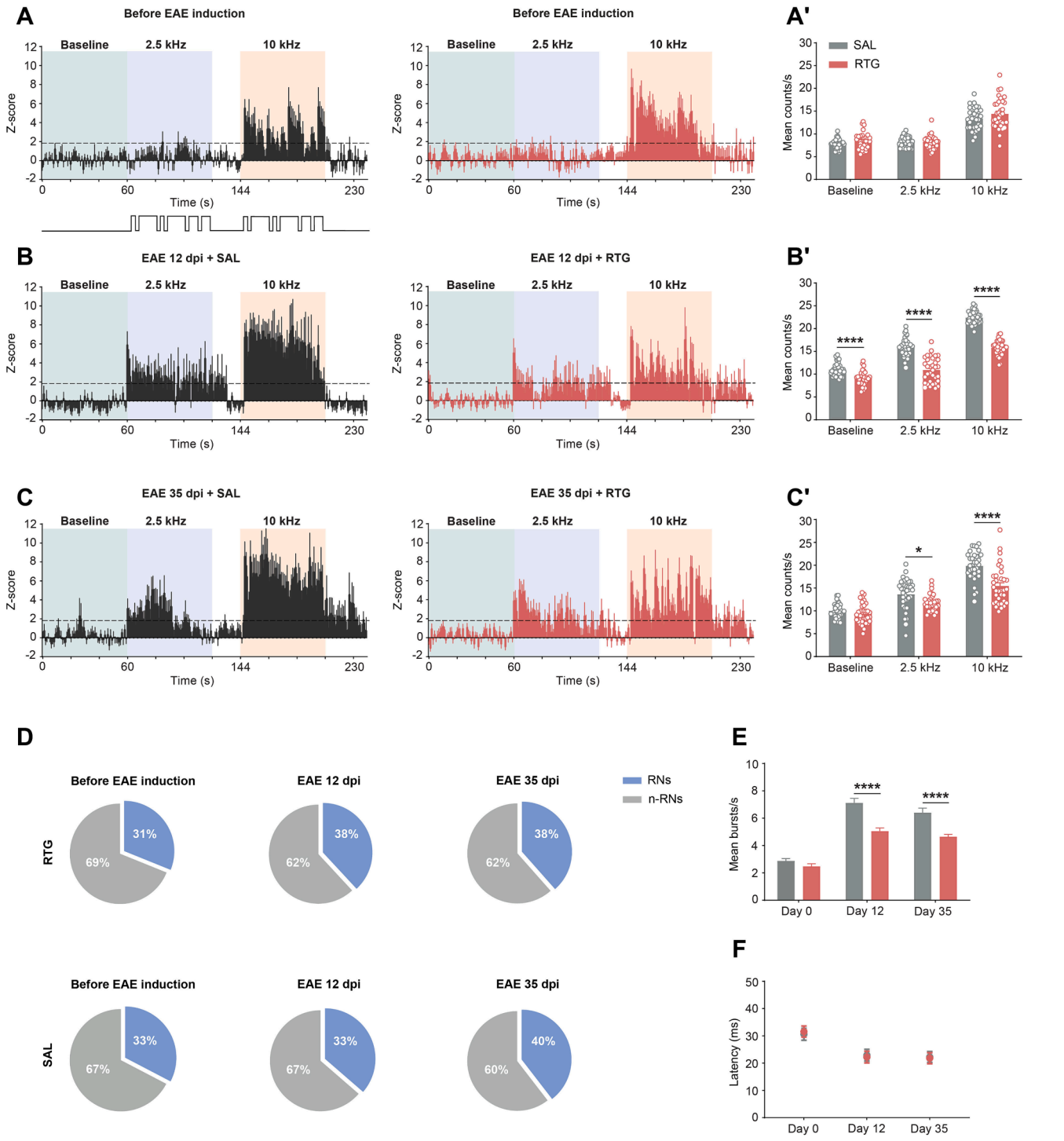

Fig. 7. Retigabine treatment reverses the impaired auditory network functionality emerging upon EAE induction. (**A, B, C**) Z-scores of auditory stimulus-evoked responses of vMGN neurons. Recordings were performed before and during the presentation of 2.5 kHz (blue insets) and 10 kHz (yellow insets) tones in EAE mice undergoing a prophylactic treatment with either saline (black) or RTG (1 mg/kg, red). Recordings obtained prior to EAE induction served as a control. (**A', B', C'**) Bar graphs indicating stimulus-related firing rates measured as baseline activity and in response to auditory stimuli of low (2.5 kHz) and high (10 kHz) frequencies (n = 34 cells from 7 SAL mice; n = 34 cells from 7 RTG mice). (**B'**) Prophylactic treatment with RTG prevented EAE-induced increased excitability at 12 (baseline, $p < 0.0001$; 2.5 kHz, $p < 0.0001$; 10 kHz, $p < 0.0001$, two-way ANOVA complemented by Šidák's test for multiple comparison). (**C'**) RTG treatment led to a significant reduction of stimulus-evoked responses 35 dpi (2.5 kHz, $p = 0.0160$; 10 kHz, $p < 0.0001$, two-way ANOVA complemented by Šidák's test for multiple comparison) (**D**) Pie charts displaying the percentage of responsive neurons (RNs) and not responsive neurons (n-RNs) to the presentation of an auditory stimulus in animals treated with either RTG or SAL. (**E**) Bar graphs showing the tendency of vMGN neurons to fire in burst mode in response to an auditory stimulus (day 12, $p < 0.0001$; day 35, $p < 0.0001$, two-way ANOVA complemented by Šidák's test for multiple comparison). (**F**) Latency of neuronal responses in the vMGN to the presentation of an auditory stimulus before (day 0) and at different stages of the EAE course (12 and 35 dpi). Data are presented as mean ± SEM; $p < 0.05$ (*), $p < 0.01$ (**), $p < 0.001$ (***), $p < 0.0001$ (****). See also Supplementary statistical analysis.

conditions, such as epilepsy. However, more ionic conductances shape the bursting properties of TC neurons, including I_M, a fast transient K^+ current (I_A), and a Ca^{2+}-activated K^+ current (I_{KCa}). The original view of bursts as all-or-none events and its functional relevance have been questioned by recent studies aimed at unraveling the information encoded in burst length and frequency (Elijah et al., 2015). In comparison to a previous study aimed at resembling the appearance of a focal demyelinating lesion (Narayanan et al., 2018), we detected an increased percentage and number of bursts, both *ex vivo* and *in vivo*. Divergences in this regard might be due to intrinsic differences in the experimental models employed (EAE vs. cuprizone, focal inflammatory vs. focal demyelinating lesion). Therefore, further investigations are required and might be complemented by behavioral readouts. In this respect, other ion channels and additional thalamic and prethalamic cell types shaping the generation of bursts in TC neurons may be influenced in the present experimental model.

Alterations in TC neuron firing pattern might reflect an impaired transmission of ascending information to the cortex. Accordingly, several recent studies shed light on the effect of general de- and remyelination processes on the activity of the thalamocortical system in experimental models of MS (Cerina et al., 2017; Narayanan et al., 2018). Notably, irreversible changes in the tonotopic organization of the auditory pathway were detected in EAE (Kapell et al., 2023) and even following complete remyelination in the cuprizone model (Cerina et al., 2018), thereby strengthening the link between altered excitability and impaired cytoarchitecture and network functionality. Noteworthy, recent studies elucidated the behavioral correlate of inflammation- and demyelination-induced altered excitability, thereby providing evidence that neural hyperactivity is accompanied by increased anxiety and reduced exploratory behavior, along with long-term memory impairment (Kapell et al., 2023; Ellwardt et al., 2018; Cerina et al., 2018). By combining *ex vivo* and *in vivo* electrophysiological approaches, we gained novel insights into an exacerbation of neuronal hyperexcitability in the neurodegenerative phase of the disease (35 dpi). Evidences indicated early neuroaxonal damage as a hallmark of MS, eventually becoming more prominent in the chronic phase of the disease (Schirmer et al., 2013). Alterations in ion channel expression and regulation robustly contribute to this phenomenon and were reported to be involved in neuroaxonal injury. We previously described impaired K^+ homeostasis at and around Nodes of Ranvier as a key mechanism to drive altered excitability in EAE (Kapell et al., 2023). Furthermore, axonal injury was attributed to diffuse distribution of several subtypes of ion channels, such as Kv1.1, Kv7, Cav2.2, Nav1.2 and Nav1.6 along chronically demyelinated neurons (Beraud et al., 2006; Kornek et al., 2001; Craner et al., 2004; Alrashdi et al., 2019; Bianchi et al., 2018; Schattling et al., 2012).

Among these players, we investigated the contribution of the K_v7 channels, with a focus on the $K_v7.3$ subunits, whose involvement in the pathogenesis of MS and respective experimental models was previously explored (Kapell et al., 2023; Hamada and Kole, 2015). Here, we precisely characterized K_v7 channel function under homeostatic and pathological conditions and explored the effect of selective pharmacological modulators, such as RTG and XE991, on TC neuron functionality by taking advantage of *Kcnq3* KO animals. We found that lack of $K_v7.3$ dramatically affected active and passive properties of TC neurons. These observations are in accordance with previous studies, indicating increased excitability and disruption of spike-frequency adaptation in mutants (Kapell et al., 2023; Gao et al., 2021; Peters et al., 2005). This feature is mediated by the activity of slow hyperpolarizing currents, such as I_M and I_{KS} (Otto et al., 2006; Schwarz et al., 2006), whose activation provides a fundamental inhibitory sink in response to trains of APs. Therefore, an aberrant spike-frequency adaptation might affect neuronal firing pattern and, hence, lead to detrimental consequences for neuronal coding. For instance, it was suggested that this biophysical property is of fundamental importance in localizing moving sounds (Goodman and Brette, 2010). Moreover, our *in vivo* investigations revealed that lack of $K_v7.3$ subunits further exacerbates vMGN TC neuron hyperexcitability, in accordance with our previous findings in A1 (Kapell et al., 2023).

I_M is mediated by different combinations of $K_v7.2$, $K_v7.3$ and $K_v7.5$ subunits (Barrese et al., 2018; Brown and Passmore, 2009), with RTG being described to have a higher affinity for heteromeric channels (Kim et al., 2015). Accordingly, significant differences between genotypes emerged when RTG-evoked currents were compared, thereby suggesting that $K_v7.3$ channels play a paramount role in mediating the RTG effect. In line with our observations, previous studies reported that mutants having *Kcnq3* deletion did not compensate by upregulating Kv7.2 channels (Kapell et al., 2023; Gao et al., 2021).

5. Conclusions

We previously showed that RTG treatment significantly mitigates disease burden in EAE animals, thereby slowing neurodegenerative processes in the chronic phase of the disease (Kapell et al., 2023). Here, we further provided evidence that a chronic, prophylactic treatment with this compound significantly reduces EAE-driven hyperexcitability, restores pre-immunization-like values and prevents alterations in thalamocortical network functionality, thereby further suggesting the use of K_v7 channel modulators as a novel neuroprotective strategy in MS and neurodegenerative disorders characterized by hyperexcitability.

6. Funding information

This work was supported by the German Research Foundation through DFG collaborative research projects (GRK 2515/1 Chembion; SFB-TRR 128/B06).

CRediT authorship contribution statement

Luca Fazio: Writing – review & editing, Writing – original draft, Visualization, Validation, Investigation, Formal analysis, Data curation, Conceptualization. **Venu Narayanan Naik:** Writing – review & editing, Visualization, Validation, Investigation, Formal analysis, Data curation. **Rajeevan Narayanan Therpurakal:** Writing – review & editing, Visualization, Investigation, Formal analysis, Data curation. **Fiorella M. Gomez Osorio:** Writing – review & editing, Visualization, Investigation, Formal analysis, Data curation. **Nicole Rychlik:** Writing – review & editing, Investigation. **Julia Ladewig:** Writing – review & editing. **Michael Strüber:** Writing – review & editing. **Manuela Cerina:** Writing – review & editing, Conceptualization. **Sven G. Meuth:** Writing – review & editing, Supervision, Project administration, Funding acquisition, Conceptualization. **Thomas Budde:** Writing – review & editing, Supervision, Project administration, Funding acquisition, Conceptualization.

Declaration of competing interest

The authors declare that they have no known competing financial interests or personal relationships that could have appeared to influence the work reported in this paper.

Data availability

The data will be made available upon reasonable request to Luca.Fazio@med.uni-duesseldorf.de.

Acknowledgements

We are thankful to Monika Wart, Jeannette Budde, and Frank Kurth for their expert technical support. We gratefully thank Heike Blum for excellent graphical illustration.

Appendix A. Supplementary material

Supplementary data to this article can be found online at https://doi.org/10.1016/j.bbi.2024.08.023.

References

Acharjee, S., et al., 2018. Reduced microglial activity and enhanced glutamate transmission in the basolateral amygdala in early CNS autoimmunity. J. Neurosci. 38 (42), 9019–9033.

Alrashdi, B., et al., 2019. Nav1.6 promotes inflammation and neuronal degeneration in a mouse model of multiple sclerosis. J. Neuroinflamm. 16 (1), 215.

Baculis, B.C., Zhang, J., Chung, H.J., 2020. The role of K(v)7 channels in neural plasticity and behavior. Front. Physiol. 11, 568667.

Barrese, V., Stott, J.B., Greenwood, I.A., 2018. KCNQ-encoded potassium channels as therapeutic targets. Annu. Rev. Pharmacol. Toxicol. 58, 625–648.

Beraud, E., et al., 2006. Block of neural Kv1.1 potassium channels for neuroinflammatory disease therapy. Ann. Neurol. 60 (5), 586–596.

Bianchi, B., Smith, P.A., Abriel, H., 2018. The ion channel TRPM4 in murine experimental autoimmune encephalomyelitis and in a model of glutamate-induced neuronal degeneration. Mol. Brain 11 (1), 41.

Bierhansl, L., et al., 2022. Thinking outside the box: non-canonical targets in multiple sclerosis. Nat. Rev. Drug Discov. 21 (8), 578–600.

Bittner, S., et al., 2013. Endothelial TWIK-related potassium channel-1 (TREK1) regulates immune-cell trafficking into the CNS. Nat. Med. 19 (9), 1161–1165.

Bosch-Bouju, C., Hyland, B.I., Parr-Brownlie, L.C., 2013. Motor thalamus integration of cortical, cerebellar and basal ganglia information: implications for normal and parkinsonian conditions. Front. Comput. Neurosci. 7, 163.

Bouafia, A., et al., 2014. Axonal expression of sodium channels and neuropathology of the plaques in multiple sclerosis. Neuropathol. Appl. Neurobiol. 40 (5), 579–590.

Brown, D.A., Passmore, G.M., 2009. Neural KCNQ (Kv7) channels. Br. J. Pharmacol. 156 (8), 1185–1195.

Budde, T., 2023. 22Biophysical Properties of Thalamic Cell Types. In: Bickford, M., Usrey, W.M., Sherman, S.M. (Eds.), The Cerebral Cortex and Thalamus. Oxford University Press.

Cain, S.M., Snutch, T.P., 2013. T-type calcium channels in burst-firing, network synchrony, and epilepsy. Biochim. Biophys. Acta 1828 (7), 1572–1578.

Calabrese, M., et al., 2009. Cortical lesions and atrophy associated with cognitive impairment in relapsing-remitting multiple sclerosis. Arch. Neurol. 66 (9), 1144–1150.

Capone, F., et al., 2020. Fatigue in multiple sclerosis: The role of thalamus. Mult. Scler 26 (1), 6–16.

Centonze, D., et al., 2009. Inflammation triggers synaptic alteration and degeneration in experimental autoimmune encephalomyelitis. J. Neurosci. 29 (11), 3442–3452.

Cerina, M., et al., 2017. The quality of cortical network function recovery depends on localization and degree of axonal demyelination. BrainBehav. Immun. 59, 103–117.

Cerina, M., et al., 2018. Protective potential of dimethyl fumarate in a mouse model of thalamocortical demyelination. BrainStruct Funct. 223 (7), 3091–3106.

Chaudhary, R., et al., 2022. Modulation of pacemaker channel function in a model of thalamocortical hyperexcitability by demyelination and cytokines. Cereb. Cortex 32 (20), 4397–4421.

Crandall, S.R., Cruikshank, S.J., Connors, B.W., 2015. A corticothalamic switch: controlling the thalamus with dynamic synapses. Neuron 86 (3), 768–782.

Craner, M.J., et al., 2004. Molecular changes in neurons in multiple sclerosis: altered axonal expression of Nav1.2 and Nav1.6 sodium channels and Na+/Ca2+ exchanger. Proc. Natl. Acad. Sci. US A 101 (21), 8168–8173.

Daldrup, T., et al., 2016. Neuronal correlates of sustained fear in the anterolateral part of the bed nucleus of stria terminalis. Neurobiol. Learn Mem. 131, 137–146.

Datunashvili, M., et al., 2018. Modulation of hyperpolarization-activated inward current and thalamic activity modes by different cyclic nucleotides. Front. Cell Neurosci. 12, 369.

Deppe, M., et al., 2016. Early silent microstructural degeneration and atrophy of the thalamocortical network in multiple sclerosis. Hum. Brain Mapp. 37 (5), 1866–1879.

Elijah, D.H., Samengo, I., Montemurro, M.A., 2015. Thalamic neuron models encode stimulus information by burst-size modulation. Front. Comput. Neurosci. 9, 113.

Ellwardt, E., et al., 2018. Maladaptive cortical hyperactivity upon recovery from experimental autoimmune encephalomyelitis. Nat. Neurosci. 21 (10), 1392–1403.

Evangelou, N., et al., 2001. Size-selective neuronal changes in the anterior optic pathways suggest a differential susceptibility to injury in multiple sclerosis. Brain 124 (Pt 9), 1813–1820.

Filippi, M., et al., 2018. Multiple sclerosis. Nat. Rev. Dis. Primers 4 (1), 43.

Gao, X., et al., 2021. Place fields of single spikes in hippocampus involve Kcnq3 channel-dependent entrainment of complex spike bursts. Nat. Commun. 12 (1), 4801.

Geurts, J.J., et al., 2012. Measurement and clinical effect of grey matter pathology in multiple sclerosis. LancetNeurol. 11 (12), 1082–1092.

Ghaffarian, N., et al., 2016. Thalamocortical-auditory network alterations following cuprizone-induced demyelination. J. Neuroinflamm. 13 (1), 160.

Gobel, K., Ruck, T., Meuth, S.G., 2018. Cytokine signaling in multiple sclerosis: lost in translation. Mult Scler 24 (4), 432–439.

Goodman, D.F., Brette, R., 2010. Spike-timing-based computation in sound localization. PLoS Comput. Biol. 6 (11).

Goverman, J., 2009. Autoimmune T cell responses in the central nervous system. Nat. Rev. Immunol 9 (6), 393–407.

Groh, A., et al., 2014. Convergence of cortical and sensory driver inputs on single thalamocortical cells. Cereb. Cortex 24 (12), 3167–3179.

Groh, A., et al., 2018. Acute and chronic pain processing in the thalamocortical system of humans and animal models. Neuroscience 387, 58–71.

Hamada, M.S., Kole, M.H., 2015. Myelin loss and axonal ion channel adaptations associated with gray matter neuronal hyperexcitability. J. Neurosci. 35 (18), 7272–7286.

Iavarone, E., et al., 2019. Experimentally-constrained biophysical models of tonic and burst firing modes in thalamocortical neurons. PLoS Comput. Biol. 15 (5).

Jukkola, P.I., et al., 2012. K+ channel alterations in the progression of experimental autoimmune encephalomyelitis. Neurobiol. Dis. 47 (2), 280–293.

Kanyshkova, T., et al., 2012. Differential regulation of HCN channel isoform expression in thalamic neurons of epileptic and non-epileptic rat strains. Neurobiol. Dis. 45 (1), 450–461.

Kapell, H., et al., 2023. Neuron-oligodendrocyte potassium shuttling at nodes of Ranvier protects against inflammatory demyelination. J. Clin. Invest.

Keith, B.J., Franklin, G.P., *Paxinos and Franklin's the Mouse Brain in Stereotaxic Coordinates, Compact.* 2019.

Kim, R.Y., et al., 2015. Atomic basis for therapeutic activation of neuronal potassium channels. Nat. Commun. 6, 8116.

Kornek, B., et al., 2001. Distribution of a calcium channel subunit in dystrophic axons in multiple sclerosis and experimental autoimmune encephalomyelitis. Brain 124 (Pt 6), 1114–1124.

Meuth, S.G., et al., 2008. Altered neuronal expression of TASK1 and TASK3 potassium channels in rodent and human autoimmune CNS inflammation. Neurosci. Lett. 446 (2–3), 133–138.

Murray, J.D., Anticevic, A., 2017. Toward understanding thalamocortical dysfunction in schizophrenia through computational models of neural circuit dynamics. Schizophr. Res. 180, 70–77.

Narayanan, V., et al., 2018. Impairment of frequency-specific responses associated with altered electrical activity patterns in auditory thalamus following focal and general demyelination. Exp. Neurol. 309, 54–66.

Oniani, T., et al., 2022. Effects of axonal demyelination, inflammatory cytokines and divalent cation chelators on thalamic HCN channels and oscillatory bursting. Int. J. Mol. Sci. 23 (11).

Otto, J.F., et al., 2006. A spontaneous mutation involving Kcnq2 (Kv7.2) reduces M-current density and spike frequency adaptation in mouse CA1 neurons. J. Neurosci. 26 (7), 2053–2059.

Peters, H.C., et al., 2005. Conditional transgenic suppression of M channels in mouse brain reveals functions in neuronal excitability, resonance and behavior. Nat. Neurosci. 8 (1), 51–60.

Rojas, J.I., et al., 2018. Thalamus volume change and cognitive impairment in early relapsing-remitting multiple sclerosis patients. Neuroradiol. J. 31 (4), 350–355.

Rychlik, N., Hundehege, P., Budde, T., 2023. Influence of inflammatory processes on thalamocortical activity. Biol. Chem 404 (4), 303–310.

Schattling, B., et al., 2012. TRPM4 cation channel mediates axonal and neuronal degeneration in experimental autoimmune encephalomyelitis and multiple sclerosis. Nat. Med. 18 (12), 1805–1811.

Schirmer, L., et al., 2013. Neuroaxonal regeneration is more pronounced in early multiple sclerosis than in traumatic brain injury lesions. BrainPathol 23 (1), 2–12.

Schwarz, J.R., et al., 2006. KCNQ channels mediate IKs, a slow K+ current regulating excitability in the rat node of Ranvier. J. Physiol. 573 (Pt 1), 17–34.

Sherman, S.M., 2001. Tonic and burst firing: dual modes of thalamocortical relay. Trends Neurosci. 24 (2), 122–126.

Shim, H.G., et al., 2018. TNF-alpha increases the intrinsic excitability of cerebellar Purkinje cells through elevating glutamate release in Bergmann Glia. Sci. Rep. 8 (1), 11589.

Suga, N., 2012. Tuning shifts of the auditory system by corticocortical and corticofugal projections and conditioning. Neurosci. Biobehav. Rev. 36 (2), 969–988.

Trimmer, J.S., 2015. Subcellular localization of K+ channels in mammalian brain neurons: remarkable precision in the midst of extraordinary complexity. Neuron 85 (2), 238–256.

Wang, J., et al., 2020. Reinforcement regulates timing variability in thalamus. Elife 9.